ULTRASOUND ASSISTED SINGLE SCREW EXTRUSION PROCESS FOR DISPERSION OF CARBON NANOFIBERS IN POLYMERS

A. I. Isayev, Changdo Jung, Kaan Gunes and Rishi Kumar
Institute of Polymer Engineering
The University of Akron
Akron, Ohio 44325-0301

Abstract

A novel method for the continuous dispersion of carbon nanofibers (CNFs) in a polymer matrix for manufacturing high performance nanocomposites was developed using an ultrasonically assisted single screw extrusion process. The effect of ultrasound on die pressure, electrical and thermal conductivity, rheological, morphological and mechanical properties of polyetherimide (PEI) filled with 1-20 wt% CNFs was studied. A reduction in the die pressure and percolation threshold of CNF/PEI composites with a permanent increase in the viscosity and a permanent decrease in $\tan\delta$ was achieved through ultrasonic treatment. Morphological studies of the treated nanocomposites revealed their improved homogeneity leading to an increase of the Young's modulus and electrical and thermal conductivity.

Keywords:

Ultrasound, Carbon nanofibers, Polyetherimide, Dispersion.

Introduction

Polymers containing CNFs have recently received a considerable attention. These nanocomposites often exhibit mechanical, electrical and thermal properties superior to conventional fiber-reinforced composites and suitable for a wide variety of potential applications [1]. Among them, CNF/polyimide nanocomposites have been studied because polyimide is one of the most reliable thermoplastic polymers for use in high temperature environment [2]. The exceptional electrical, mechanical and thermal properties of CNFs along with their light weight positioned them for electronic structures, electro-statically dissipative materials, polymer nanocomposites and biological systems [1]. The CNF's are produced by vapor grown carbon method, based on the catalytic decomposition of hydrocarbons in the vapor phase at 500-1500^{o}C [3]. However, as result of manufacturing process, CNFs are easily aggregated and bundle together or entangled due to strong interfiber attraction which is the main obstacle for their use in many applications [4]. Currently, the biggest challenge for the effective use of CNFs is the lack of their dispersion in the polymer matrix.

The commonly used methods to disperse CNFs are mechanical, melt processing and plasma treatment **[5-7]**. Among these methods ultrasonication of CNFs in solutions for a prolonged time (minutes and hours) is one of the most commonly used methods for their dispersion [8]. This is a batch process that is typically carried out in an ultrasonic bath. However, the prolonged ultrasonication introduces defects in CNFs by shortening them and hence resulting in the reduced aspect ratio which is responsible for many of their attractive properties [9]. Also, melt processing of the high viscosity polymer/CNF mixtures is utilized using high shear mixing in extruder [5,10-15] and internal mixer [5, 16-19]. These methods have advantages as they are solvent free processes. Plasma coating is also used to enhance the dispersion of the CNFs in the polymer

matrix [7]. In-situ polymerization is also one of the methods used to keep bundles of CNFs dispersed in the polymer matrix [20]. As reviewed in [21], some other methods have been attempted for enhancing dispersion, like in-situ production of CNFs, but found a limited success.

Recently, use of high power ultrasound in extrusion process was proposed to disperse nanosize fillers in polymers at the residence time of the ultrasonic treatment of a few seconds. In particular, it was found that ultrasound assists in better silica filler dispersion in rubber [22] and nanoclay intercalation and exfoliation in polypropylene [23, 24] and polyethylene [25] matrices in a extrusion process.

The present study describes preparation of CNF/PEI nanocomposites obtained by means of an extrusion process in a novel ultrasonic reactor. Mechanical, electrical, and thermal properties and rheology of the obtained nanocomposites were studied. Effects of the processing parameters on dispersion of CNFs in PEI were elucidated.

Experimental

Materials

CNFs, Pyrograf-III, PR-19-HT, were provided by Applied Sciences, Inc., Cedarville, OH. These nanofibers are vapor grown and subsequently heated to temperatures up to 3000^{o}C to increase their electrical conductivity. The diameter of the CNFs was varied from 70 to 200 nm and the length was between 50 and 100 μm. The CNFs were used without any further purification. PEI, Ultem 1000P, in powder form from GE Plastics was used as received. Resin T_g is 217^{o}C, with a powder particle diameter of 350 μm. Molded products have transparent amber brown color. Chemical structure of PEI is:

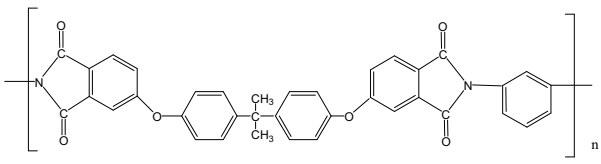

The PEI powder was dry-mixed at various CNF contents by ball milling for 24 hrs. The mixture was then dried under vacuum at 120^{o}C for a minimum of 24 hrs prior to processing.

Ultrasonic Extruder

A single screw ultrasonic compounding extruder having a screw diameter of 25.4 mm and L/D ratio of 33:1 was used. It was built based on a Killion extruder with L/D of 24. Three mixing sections and the ultrasound treatment zone were made along the barrel. A schematic drawing of the ultrasound extruder is shown in Figure 1.

Two 6 kW ultrasonic power supplies were connected to two converters to generate ultrasonic waves at a frequency of 20 KHz. Each converter was connected in series to a 1:1 booster and a water-cooled titanium horn, which was inserted into the barrel. The tip of the ultrasonic horn was in contact with the molten compound. The amplitude of ultrasound was varied from 5 to 15 μm. This allowed us to study the effect of increasing ultrasound power on the dispersion of CNFs in PEI melt.

The barrel surface in the ultrasound treatment zone was streamlined in such a way that the compound melt was forced to flow in gaps between the horns and the screw. This prevented creation of a dead zone in the flow domain. The mean residence time in the ultrasonic treatment zone was 7 s at a flow rate of 15 g/min.

Cylindrical ultrasound horns of 25.4 mm diameter were used. The horns were provided with curved tips to match the curvature of the barrel surface. They were precisely aligned with the curvature of the barrel to maintain a constant gap thickness. The gap opening for the flow of compound in ultrasonic zone was kept at 2.54 mm. Seals made of 40% graphite filled Vespel® were used to prevent the flow of melt along the lateral clearance between the barrel and horn in

the ultrasound treatment zone. A pressure transducer was mounted on the barrel before the ultrasonic treatment zone, as shown in Figure 1.

The barrel temperature of the ultrasonic extruder was controlled by several heaters connected to temperature controllers. Three temperature control zones were located on the original extruder within the conveying, compression and metering sections. In the ultrasonic barrel attachment following the original extruder, four additional temperature control zones were made available. Zone 1 was located at the transition region from the original extruder to the ultrasonic attachment. It had one heater controlled by the shim stock thermocouple. Zone 1 also had a nozzle thermocouple monitoring the melt temperature. Feedback from nozzle type thermocouple was used to control the temperature in zone 2. Zone 2 had one heater located at the end of the mixing section within the ultrasonic treatment zone. Temperature of Zone 3 was controlled using the nozzle type thermocouple. Shim stock thermocouple was used to control the temperature in zone 4, corresponding to the die section.

The extruder screw had a variable diameter along its length. The total length of the screw was 838 mm. The diameter of the screw was 25.4 mm for the first 624.5 mm, corresponding to the extruder mixing section before the ultrasonic treatment zone. Before the ultrasonic treatment zone, the screw diameter was enlarged to 38.1 mm till location of the pressure transducer. The length of this section was 60.2 mm. Following this section, the diameter of the extruder screw was reduced to 33.0 mm. This section had no flights in the vicinity of the horns in order to provide the 2.54 mm gap for ultrasonic treatment. The length along this section was 85.1 mm. The diameter of the screw after the ultrasound horns was 25.4 mm.

The extruder screw had Union Carbide (UCM) and Melt Star mixing sections along the screw before the ultrasonic treatment zone and another Melt Star mixing section at the end of the screw

just before the die, as shown in Figure 1. The UCM section was 53.8 mm long, while both Melt Star mixing sections were 63.5 mm long. A converging circular die with exit diameter of 3.0 mm was connected to the extruder. The die diameter converged from 25.4 mm to 3.0 mm along a length of 51.7 mm and after that it maintained at 3.0 mm diameter along a length of 12.7 mm.

Nanocomposite Preparation

PEI/CNF nanocomposites of various CNF contents (3, 5, 8, 11, 15, and 20 wt%) were prepared by a single screw ultrasonic extruder with and without ultrasonic treatment. The extrusion temperature was varied from 320 to 340°C from the feed zone to the die. The screw speed was 30, 60 and 100 rpm. Flow rate was 15 g/min. The ultrasonic treatment was carried out at amplitudes of 5, 7.5, 10 and 15 μm. Extrudates were quenched in a room temperature water bath and then pelletized. Unfilled PEI was also processed using the same procedure, to produce a control sample.

SEM Studies

The quality of the mixing is an important parameter to quantify dispersion of CNFs. Therefore, microscopic analysis was conducted by means of a scanning electron microscopy (SEM) to identify the level of dispersion of CNF's in melt at different processing conditions. The morphologies of samples were observed using Hitachi S-2150 SEM at 20kV. For this purpose, injection and compression molded specimens were prepared. The specimens were cold fractured in liquid nitrogen. The fractured surfaces were sputter coated with silver.

To determine the CNF's aspect ratio in the composites, selected CNF/PEI nanocomposites were dissolved in N-methyl-2-pyrrolidinone. The solution was filtered through a poly(tetrafluoroethylene) membrane disk filter (Gelman, 0.2 mm pore size) to separate CNFs.

Afterwards, CNFs were washed several times with N-methyl-2-pyrrolidinone to completely remove the residual polymer. CNFs removed in this process were observed using the SEM.

Rheological Measurements

An Advanced Rheometric Expansion System (ARES, Rheometrics Scientific) was used in the dynamic mode with parallel fixtures of diameter of 25 mm and a gap of 2 mm. The storage, G', and loss, G", moduli were obtained at a fixed strain of 2% in dynamic frequency sweep experiments as a function of an angular frequency, ω, ranging from 0.1 to 100 rad/s at a 340^{o}C temperature. Data acquisition was carried out with the aid of a microcomputer interfaced with the rheometer. All experiments were conducted under nitrogen environment to prevent oxidation of the samples.

Measurement of Tensile Properties

Specimens for tensile tests (ASTM D638) were prepared by a HAAKE mini-jet piston injection molding machine. Injection molding was carried out at a melt temperature of 340°C and a mold temperature of 120°C. Pellets of a total weight of 6 g were loaded into the cylinder and melted for 180 s to make 2 g dumbbell shaped samples. The injection pressure was 65 MPa in each case.

Instron tensile testing machine (Model 5567, Instron Corp.) was used to carry out tensile tests at room temperature. The ASTM D638 method was followed. Samples were clamped in the jaws of the testing machine and put under tension at a crosshead speed of 5 mm/min. A 30 kN load cell was used to register the force values against displacement. An extensometer with 7.62 mm gauge length was used to record the displacement data. For each condition, a minimum of 5 specimens were tested. The yield stress, yield strain, stress at break, strain at break, Young's

modulus and toughness (area under the stress-strain curve) were measured. The average and standard deviation of these values were calculated.

Conductivity Measurements

The resistivity of an insulator can be measured by using a power source of known voltage by measuring the resulting current, and calculating the resistivity according to the Ohm's law. The resistivity is calculated from the value of resistance and the physical dimensions of the test sample. Disks with a thickness of 1 mm and a diameter of 60 mm were prepared by compression molding. An electrometer, Keithley Instrument Model No.6517A, attached to an 8009 test fixture was used to measure the volume resistivity of the sample in accordance with ASTM D257 method. A constant voltage of 10V was applied for 60 s in the test. It should be noted that the application of higher voltages led to different values of resistivity (conductivity). Moreover, at high loadings of CNFs, resistivity readings became unstable and electrometer got tripped off.

Results and Discussion

Process Characteristics

The entrance pressure and temperature of the ultrasonic treatment zone as a function of ultrasonic amplitude is presented in Figure 2. It is seen that the overall level of the entrance pressure during this process is very low (below 1 MPa). The entrance pressure of the ultrasonic treatment zone is substantially reduced as the ultrasonic amplitude is increased leading to improved processability of melts. This decrease of pressure was previously explained as a result of acoustic cavitation leading to permanent and thixotropic changes in the melt [26]. The degradation of polymer chains during ultrasonic treatment may become more pronounced in the presence of CNFs. This may lead to permanent reduction of matrix viscosity, as already indicated by the observed slight reduction of viscosity of pure PEI after the treatment. In addition,

ultrasonic waves may also enhance shear thinning behavior of the melt leading to a temporary decrease of melt viscosity that recovers after treatment (thixotropic effect). It is also noted from Figure 2 that the temperature at the ultrasonic treatment zone increases with increasing ultrasonic amplitude. This behavior can be attributed to the effect of energy dissipation of the ultrasonic wave in a viscoelastic melt causing melt temperature rise by conversion of mechanical ultrasonic energy to thermal energy. In addition to heating effect, reduced friction of polymer melt along horn surfaces due to ultrasonic vibrations may also lead to decrease in die pressure.

It is also evident from Figure 2 that the pressure increases with increasing CNF concentration. It is interesting to note that the pressure is increased linearly up to 8 wt% CNF loading. This linear increase of pressure slows down at 11 wt% (for the purpose of clarity these data were not shown in Fig. 2) and 15 wt% loading. Then a significant increase of pressure was observed at 20 wt% CNF content, suggesting a possibility of formation of interconnected network of CNFs. Such a behavior can be attributed to the presence of the rheological percolation threshold in the melt between 15 and 20 wt% loading of CNFs under ultrasonic treatment.

Figure 3 presents ultrasonic power consumption during ultrasonic treatment of PEI containing 3 wt% (a) and 11 wt% (b) of CNFs as a function of ultrasonic amplitude at different screw rotation speeds. The measured power consumption is the total power that is consumed due to oscillations of the horn and propagation of ultrasonic waves in the polymer melt leading to heat dissipation. Unfortunately, the power loss due to the heat dissipation and power used by ultrasonic wave propagation through the melt cannot be separated. The only energy losses that can be measured are the initial power consumption when horn works without any loading. The results presented in Fig. 3 are obtained after subtracting of these losses from total power

consumption. It is seen that the power consumption increases with increasing ultrasonic amplitude. The power consumption is also seen to continuously increase as screw rotation speed decreases. This is due to an increase of the pressure at lower rotation speeds. The latter is due to the fact that a decrease of the screw rotation speed leads to a lower shear rate in the melt causing an increase of its viscosity.

The ultrasonic power consumption during ultrasonic treatment of PEI at various CNF concentrations as a function of ultrasonic amplitude is shown in Figure 4. This set of data is obtained at 60 rpm. On increasing the CNF content from 0 to 20 wt%, an increase of the power consumption was observed with an increase of amplitude. An increase of power consumption with CNF concentration is evidently due to the higher energy required to disperse CNFs in melt [23].

Rheology

Figure 5 shows the dependence of complex viscosity at 0.2 s^{-1} frequency on ultrasonic amplitude at various screw rotation speeds for PEI containing 3 wt% of CNFs. It is observed that the complex viscosity of the composites processed at rotation speeds of 30 rpm and 60 rpm reach their maximum values at an amplitude 10 μm. The presence of the viscosity maximum is a result of a competition between the viscosity increase due to the increased surface area with better dispersion of CNFs at higher amplitude and the viscosity decrease due to a possible breakup of molecular chains by high power ultrasound during melt extrusion [22]. The viscosity of material at rotation speed of 100 rpm decreases with increasing ultrasonic amplitude and does not show a maximum. This is because the degradation of polymer is apparently dominates at the higher rotation speed leading to the viscosity reduction. In addition, the observed viscosity reduction is due to the breakage of CNFs which is more pronounced at the higher rotational speed, as

indicated by the microscopic analysis (see Fig. 15a). As shown below, viscosity of ultrasonically treated pure PEI is reduced only slightly. However, due to the presence of CNFs and multiple interfaces in nanocomposites, it is expected that PEI matrix degradation would be more enhanced.

Figure 6 shows the complex viscosity (a) and $\tan\delta$ (b) as a function of frequency for the untreated and ultrasonically treated CNF/PEI nanocomposites containing 0 to 20 wt% CNFs. It is clear that the viscosity of CNF/PEI composites increases (Fig. 6a) while tan δ decreases (Figure 6b) with increasing CNF content. Viscosity of ultrasonically treated composites is consistently higher compared to that of untreated ones. In contrast, tan δ of treated nanocomposites is significantly lower than those untreated ones. Also, the curve becomes more flat in the low frequency region indicating that CNFs affect the relaxation behavior of polymer chains such that the storage modulus increases more with ultrasonic treatment than the loss modulus (see Figure 8). This results in lowering tan δ of nanocomposites. This is possibly due to an improved dispersion of the treated CNF/PEI nanocomposites, as indicated by the SEM studies reported below. At the same time, viscosity of virgin PEI slightly decreases with ultrasonic treatment. This is due to a possible breakup of macromolecular chains during melt extrusion. The viscosity of nanocomposites obtained at an amplitude of 10 μm shows slightly lower values than those at amplitudes of 5 μm and 7.5 μm. This is not only because of the thermomechanical degradation of polymer, but also because of a possibility of breakage of nanofibers during ultrasonic treatment. This explanation is supported by experimental results of the length of CNFs extracted from composites, as shown below (see Figure 15). This observation is also in agreement with values of the Young's modulus of nanocomposites containing 11 wt% of CNFs, also indicated below (see Figure 17b). As seen in Figure 6, viscosity of the composites exhibit more frequency

dependence at low frequencies (in the range from 0.1 to 1 s^{-1}) as the CNF concentration is increased. Also, such a strong frequency dependence and, therefore, shear thinning is especially pronounced for ultrasonically treated composites at concentrations of 15 and 20 wt%. This strong shear thinning behavior can be attributed to a greater degree of polymer-CNF interactions and due to better dispersion of the CNFs and formation of continuous CNF network. Also, a steep rise in viscosity for treated nanocomposites at concentration above 15 wt% is an indication of rheological percolation threshold. This can be better understood by plotting complex viscosity vs. CNFs concentration at a frequency of 0.2 s^{-1}, as shown in Figure 7. From this figure it is difficult to judge the presence of rheological percolation threshold for untreated nanocomposites at the concentration range studied. Possibly, the percolation threshold lies at higher concentration. Therefore, this suggests that ultrasonic treatment leads to the reduction of the rheological percolation threshold in nanocomposites. It means that the viscosity curve is a possible tool for identifying the presence of the percolation threshold for these composites, as earlier shown in [19]. This percolation threshold is evidently created by a better dispersion of CNFs by ultrasonic treatment.

The effect of ultrasound on dispersion of CNFs can also be seen from an increase in the storage and loss moduli for the treated composites (Fig. 8). Both the storage and loss moduli increase with ultrasonic amplitude and CNFs content with more effect seen in G' than in G". The value of G' also increases with frequency. However, the effect is more pronounced at low frequencies, as compared to high frequencies. Based on these data one can conclude that nanocomposites at CNF concentrations above 15 wt% exhibit a dramatic increase in the storage modulus with ultrasonic treatment, indicating an existence of the rheological percolation threshold. Furthermore, the effect of CNFs and ultrasonic treatment on the structural differences

between polymer and nanocomposites can be seen from the logarithmic plot of G' vs. G" (Fig. 8c), which is similar to so-called Cole-Cole plot [27]. Such a plot was used by many researchers [28,29] to study the dynamic properties of materials in the melt state. From Fig. 8c it is clear that at given G" value, G' increases more significantly with CNF content. This is in accordance with behavior reported for PC/MWNT nanocomposites [30]. Clearly, ultrasonically treated composites show increase in G' at given G" for all CNFs loadings indicating a stronger network structure due to the better dispersion of CNFs in a polymer matrix.

Electrical and Thermal Conductivity

The electrical conductivity of composites is generally dependent on the carbon fiber volume fraction. At low fiber loadings, the conductivity of the composite is still very close to that of the pure insulating polymer matrix. At some critical loading, corresponding to the electrical percolation threshold, the conductivity increases by several orders of magnitude with very little increase in the fiber amount. At the percolation threshold, fibers begin to form continuous conductive networks throughout the composite and conductivity increases sharply. After this drastic increase, the conductivity once again levels off and assumes values close to that of the conductive particles.

Figure 9 shows electrical volume resistivity (a) and thermal conductivity (b) of nanocomposites as a function of CNF concentration. For ultrasonically treated composites, the resistivity at the 15 wt% of CNFs loading dropped by about 2 orders of magnitude. At the same time, a similar drop in the resistivity of composite extruded without ultrasonic treatment occurs at 17 wt% CNF loading. Evidently, these concentrations correspond to the onset of percolation with and without ultrasonic treatment. Volume resistivity is dependent not only on fiber

concentration, but also on fiber length and dispersion. Evidently, high power ultrasonic treatment leads to better interconnected network of CNFs with improved dispersion of CNF even with reduction in aspect ratio of CNFs. Both these effects are indicated by the results shown below. Clearly, the ultrasonic amplitude has an effect on the electrical percolation threshold. The results for electrical percolation threshold of treated nanocomposites are in agreement with rheological percolation threshold. It was observed that both fall in between the 15 and 20 wt % of CNFs concentration. In earlier studies on PP/CNF [19] and PC/MWNT [30] nanocomposites, prepared by melt processing, it was observed that both rheological and electrical percolation lies in the same range. However, in some other studies [31, 32] concentrations corresponding to rheological and electrical percolation threshold have found to be different, with electrical percolation values being higher than the rheological one.

The aspect ratio of the CNFs also plays an important role on the concentration of fibers necessary to achieve percolation. It is seen from Figure 9a that composites prepared by ball milling show percolation threshold at much lower CNF concentration (4 wt %). This is due the presence of long and aggregated fibers in these composites.

The thermal conductivity of PEI/CNF nanocomposites increases from 0.23 to 0.52 W/mK as the CNF concentration increases from 5 wt% to 20 wt% (Figure 9b). The thermal conductivity of CNFs is 20 W/mK, as reported by Applied Sciences, Inc. Although the thermal conductivity increases by more than two times with the addition of the CNFs, the prepared nanocomposites do not show a percolation threshold based on these measurements. This is because heat transport mainly occurs through the polymer matrix at fiber concentrations used. It is interesting to note that the thermal conductivity of 20 wt% CNF/PEI composites increases with increasing

ultrasonic amplitude. This observation could be a result of the continuously improved dispersion of CNFs by increasing ultrasonic power consumption.

Microscopic Analysis

Figure 10a shows SEM micrographs of CNFs as received. This figure indicates the presence of bundles of CNFs. As received CNFs have large aspect ratios (> 100) with diameters varying from 70 nm to 200 nm. Size of CNF bundles is seen to be in the range from 10 μm to 50 μm. Some catalyst impurity and amorphous carbon may also be present in these samples [19]. After ball milling of CNFs with PEI powder and subsequent molding, the CNF bundles still remain in molding, as shown in Fig. 10b. Therefore, a poorly dispersed mixture is obtained. Interwoven bundles and aggregates of CNFs up to 50 μm in size were observed in SEM micrographs (Fig. 10b). These bundles of entangled CNFs make the dispersion of the fibers into the polymer matrix more difficult. However, as seen in Figure 9a, these aggregates help to induce electrical conductivity due to easier charge transfer along bundles of CNFs, due to longer fiber length and better interconnected fiber network [33]. Possibly, if the extrusion process can be carried out without a breakage of CNFs along with improved dispersion, one would observe a lower electrical percolation threshold.

To evaluate the dispersion of CNFs in a PEI matrix, examination of the surface of injection molded samples broken in the liquid nitrogen was carried out by SEM. In particular, Figure 11 shows the SEM micrographs of fractured surface of the 3 wt% CNF/PEI nanocomposites before and after ultrasonic treatment at amplitude of 10 μm. It cannot be visually verified at this concentration if CNFs are better dispersed in PEI matrix after ultrasonic treatment since the CNFs at this low concentration are already dispersed very well throughout the samples even without ultrasonic treatment. Free individual fibers are clearly seen from SEM micrographs.

They are apparently not wetted by the polymer due to poor adhesion and fiber-matrix interaction. This observation is in agreement with results on the strength of PEI/CNF nanocomposites which do not vary with increasing CNFs loading, as shown below.

Figures 12 and 13 depict SEM micrographs of fractured surfaces of the 15 wt% and 20 wt% CNF/PEI nanocomposites without and with ultrasonic treatment at an amplitude of 10 μm. There is a higher possibility of overlapping of fibers throughout the PEI matrix at 20 wt% CNF composition compared to 15 wt % of CNF content. The CNFs are clustered in the matrix with about 2~5 μm diameter in untreated composites and resin rich part without CNFs is also evident, as indicated by arrows. There is a sharp contrast between the resin clumps without and with fibers. In the treated nanocomposites, CNFs are not clustered but still in contact with each other. The latter could be the reason why the percolation threshold is achieved at a concentration of about 15 wt% in ultrasonically treated nanocomposites.

Figure 14 shows the SEM micrograph of CNFs extracted from the nanocomposite. As seen from this figure, fiber length is significantly reduced from the initial length of 30~100 μm reported by Applied Sciences, Inc. to 2~10 μm. The degradation of fiber length is not only attributed to the high shear in extruder [21] but also to the action of high power ultrasound. In particular, Figure 15 shows the length distribution of CNFs in nanocomposites obtained without and with ultrasonic treatment, respectively. In Figure 15a, effect of screw rotation speed is presented in the absence of ultrasound. With screw rotation speed, the longer fibers are broken. This is caused by higher stresses acting at high screw rotation speed. The average value of CNF length at 30 rpm is found to be 5.4 μm. At 60 rpm this length is decreased to 4.4 μm. Another factor considered in assessing fiber damage was the effect of ultrasound. Figure 15b shows length distribution of CNFs in nanocomposites obtained without and with ultrasonic treatment at

a screw rotation speed of 60 rpm. Only slight decrease in the fiber length due to ultrasonic treatment is observed.

Mechanical Properties

Typical stress-strain curves of the PEI/CNF composites at various CNF contents ultrasonically treated at an amplitude of $5\,\mu m$ are presented in Figure 16a. As the CNF concentration is increased, the nanocomposites become more brittle. At concentrations above 11 wt%, the PEI/CNF nanocomposites exhibit no yielding behavior indicating a lower toughness with increase CNF concentration. It is also seen that the Young's modulus of the nanocomposites significantly increases with increasing CNF concentration.

The stress-strain curves of PEI/CNF nanocomposites containing 11wt% CNFs ultrasonically treated at various amplitudes are given in Figure 16b. The yield stress is not affected by ultrasonic treatment, while the elongation at break is reduced. The reduction in elongation at break and toughness with ultrasonic treatment is possibly due to the scission of polymeric chains at high ultrasonic amplitude resulting in increased brittleness of material. As PEI/CNF nanocomposites do not yield at high levels of CNF loading, the terms the yield stress and strength are used interchangeably in this study. The strength of PEI/CNF nanocomposites showed little change with ultrasonic treatment and CNF concentration (Figure 17a). It is seen from Figure 17a that the strength of nanocomposites does not change up to 15% loading and then slightly decreases. This behavior is attributed to the lack of adhesion between CNFs and PEI matrix. The explanation is supported by the detachment of fibers seen in SEM micrographs depicted in Figure 11. The average values of mechanical properties of PEI/CNF composites are summarized in Table 1 along with the standard deviation in measurements. Figure 17a also

shows the strength of composites obtained after ball milling. These composites indicate inferior values of the strength in comparison with those of extruded composites.

Ultrasonic treatment at amplitude of 5 and 7.5 μm leads to an increase in the Young's modulus of the nanocomposites, as can be seen from Figure 17b. The modulus of PEI/CNF nanocomposites containing 11 and 15 wt% CNFs is increased by 17% and 13%, respectively, upon ultrasonic treatment at an amplitude of 5 μm. Figure 17b also shows values of the modulus of samples after ball milling. The values of modulus of these nanocomposites are typically lower than those of extruded nanocomposites.

Conclusions

CNF/PEI nanocomposites with contents up to 20 wt% have been prepared by means of an ultrasonic single screw compounding extruder. Based on rheological and electrical conductivity measurements, the estimated percolation threshold in ultrasonically treated CNF/PEI nanocomposites is found to be at about 15 wt% of CNF loading which is lower than those of untreated nanocomposites showing the higher percolation threshold. Furthermore, it was established that high power ultrasound is effective in obtaining relatively homogeneous dispersion with improved electrical and thermal conductivity in the CNF/PEI nanocomposites, in comparison with extruded untreated ones. However, the sample prepared by ball milling and without extrusion showed much lower electrical percolation threshold.

An increase of the Young's modulus in CNF/PEI nanocomposites was recorded under ultrasonic treatment, without reduction in the tensile strength up to 15 wt% CNF loading. A decrease in the tensile strength at higher loadings is attributed to the lack of adhesion between the CNFs and PEI matrix.

SEM micrographs of dry-mixed PEI/CNF composites by ball milling indicated the presence of CNF bundles. However, the CNF bundles are absent after compounding using an ultrasonic single screw extruder with ultrasonic treatment indicating good dispersion of CNFs in PEI matrix. SEM micrographs of fibers extracted from nanocomposites show a breakage of the CNFs during extrusion. The breakage is strongly affected by the screw rotation speed and slightly affected by ultrasonic amplitude.

Acknowledgements

This work was supported by the Division of Engineering of the National Science Foundation (CMMI-0654326) and partially by the NASA Headquarters (NNL05AA33C). Authors wish to thank Dr. Sayata Ghose of the NASA Langley for providing the thermal conductivity data.

References

1. Ajayan, P. M., Schadler, L. S., and Braun, P. V., Nanocomposite Science and Technology, Weinheim, Wiley, 2003
2. Hergenrother, P. M., The use, design, synthesis, and properties of high performance/high temperature polymers: An overview, High Performance Polymers, 2003; 15: 3-45.
3. Mordkovich, V. Z., Carbon nanofibers: A new ultrahigh-strength material for chemical technology, Theoretical Foundations of Chemical Engineering (Translation of Teoreticheskie Osnovy Khimicheskoi Tekhnologii), 2003; 37: 429-438.
4. Johnson, J. A., Barbato, M. J., Hopkins, S. R., and O'malley, M. J., Dispersion and film properties of carbon nanofiber pigmented conductive coatings, Progress in Organic Coatings, 2003; 47: 198-206.
5. Ma, H., Zeng, J., Realff, M. L., Kumar, S., and Schiraldi, D. A., Processing, structure, and properties of fibers from polyester/carbon nanofiber composites, Composites Science and Technology, 2003; 63: 1617-1628.
6. Brandl, W., Marginean., G., Functionalization of the carbon nanofibers by plasma treatment, Thin Solid Films, 2004; 447-448 : 181-186.
7. Shi, D., Lian, J., He, P., Wang, L. M., Xiao, F., Yang, L., Schulz, M. J., and Mast, D. B., Plasma coating of carbon nanofibers for enhanced dispersion and interfacial bonding in polymer composites, Applied Physics Letters, 2003; 83: 5301-5303.
8. Zhao, J., Schaefer, D. W., Shi, D., Lian, J., Brown, J., Beaucage, G., Wang, L., and Ewing, R. C., How Does Surface Modification Aid in the Dispersion of Carbon Nanofibers? Journal of Physical Chemistry B, 2005; 109: 23351-23357.

9. Gauthier, C., Chazeau, L., Prasse, T., and Cavaille, J. Y., Reinforcement effects of vapour grown carbon nanofibres as fillers in rubbery matrices, Composites Science and Technology, 2005; 65: 335-343.

10. Carneiro, O. S., Covas, J. A., Bernardo, C. A., Caldeira, G., Van Hattum, F. W. J., Ting, J. M., Alig, R. L., and Lake, M. L., Production and assessment of polycarbonate composites reinforced with vapor-grown carbon fibers, Composites Science and Technology, 1998; 58: 401-407.

11. Hammel, E., Tang, X., Trampert, M., Schmitt, T., Mauthner, K., Eder, A., and Potschke, P., Carbon nanofibers for composite applications, Carbon, 2004; 42: 1153-1158.

12. Kuriger, R. J. and Alam, M. K., Extrusion conditions and properties of vapor grown carbon fiber reinforced polypropylene, Polymer Composites, 2001; 22: 604-612.

13. Kuriger, R. J., Alam, M. K., Anderson, D. P., and Jacobsen, R. L., Processing and characterization of aligned vapor grown carbon fiber reinforced polypropylene, Composites, Part A: Applied Science and Manufacturing, 2001; 33A: 53-62.

14. Hine, P., Broome, V., and Ward, I., The incorporation of carbon nanofibers to enhance the properties of self reinforced, single polymer composites, Polymer, 2005; 46: 10936-10944.

15. Zeng, J., Saltysiak, B., Johnson, W. S., Schiraldi, D. A., and Kumar, S., Processing and properties of poly(methyl methacrylate)/carbon nanofiber composites, Composites, Part B: Engineering, 2004; 35B: 245-249.

16. Lozano, K. and Barrera, E. V., Nanofiber-reinforced thermoplastic composites. I. Thermoanalytical and mechanical analyses, Journal of Applied Polymer Science, 2000; 79: 125-133.

17. Yang, S., Lozano, K., Lomeli, A., Foltz, H. D., and Jones, R., Electromagnetic interference shielding effectiveness of carbon nanofiber/LCP composites, Composites, Part A: Applied Science and Manufacturing, 2005; 36A: 691-697.

18. Lozano, K., Yang, S., and Zeng, Q., Rheological analysis of vapor-grown carbon nanofiber-reinforced polyethylene composites, Journal of Applied Polymer Science, 2004; 93: 155-162.

19. Lozano, K., Bonilla-Rios, J., and Barrera, E. V., A study on nanofiber-reinforced thermoplastic composites (II): investigation of the mixing rheology and conduction properties, Journal of Applied Polymer Science, 2001; 80: 1162-1172.

20. Higgins, B. A. and Brittain, W. J., Polycarbonate carbon nanofiber composites, European Polymer Journal, 2005; 41: 889-893.

21. Breuer, O. and Sundararaj, U., Big returns from small fibers: A review of polymer/carbon nanotube composites, Polymer Composites, 2004; 25: 630-645.

22. Isayev, A. I., Hong, C. K., and Kim, K. J., Continuous mixing and compounding of polymer/filler and polymer/polymer mixtures with the aid of ultrasound, Rubber Chemistry and Technology, 2003; 76: 923-947.

23. Lapshin, S. and Isayev, Continuous process for melt intercalation of PP-clay nanocomposites with aid of power ultrasound, J. Vinyl Additive Technol., 2006, 12, 78-82.

24. Lapshin, S. and Isayev, A. I., Ultrasonic aided extrusion process for preparation of polypropylene-clay nanocomposites, J. Vinyl Additive Technol., 2007; 13: 40-45.

25. Swain, S. K. and Isayev, A. I., Effect of ultrasound on HDPE/clay nanocomposites: Rheology, structure and properties, Polymer, 2007; 48: 281-289.

26. Isayev, A. I., Wong, C. M., and Zeng, X., Effect of oscillations during extrusion on rheology and mechanical properties of polymers, Advances in Polymer Technology, 1990; 10: 31-45.

27. Cole, K.S., Cole, R.H., Dispersion and absorption in dielectrics I . Alternating current characteristics, 1941; 9: 341-351.

28. Han, C.D., Kim, J., Kim, J.K., Determination of the order- disorder transition temperature of block copolymers, Macromolecules, 1989; 22: 383-394.

29. Chuang, H.K., Han, C.D., Rheological behavior of polymer blends, Journal of Applied Polymer Science, 1984; 29: 2205-2229.

30. Potschke, P., Fornes, T.D., Paul, D.R., Rheological behevior of multiwalled carbon nanotube/polycarbonate composites, Polymer, 2002; 43: 3247-3255.

31. Hu, G., Zhao, C., Zhang, S., Yang, M., Wang, Z., Low percolation threshold of electrical conductivity and rheology in poly(ethylene terephtalate) through the networks of multi-walled carbon nanotubes, Polymer, 2006; 47: 480-488.

32. Du, F., Scogna, R.C., Zhou, W., Brand, S., Fischer, J.E., Winey, K.I., Nanotube networks in polymer nanocomposites: Rheology and electrical conductivity, Macromolecules, 2004; 37: 9048-9055.

33. Jimenez, G. A. and Jana, S. C., Preparation of PEEK and carbon nanofiber composites by chaotic mixing, SPE ANTEC Technical Papers, 2005; 63rd: 1938.

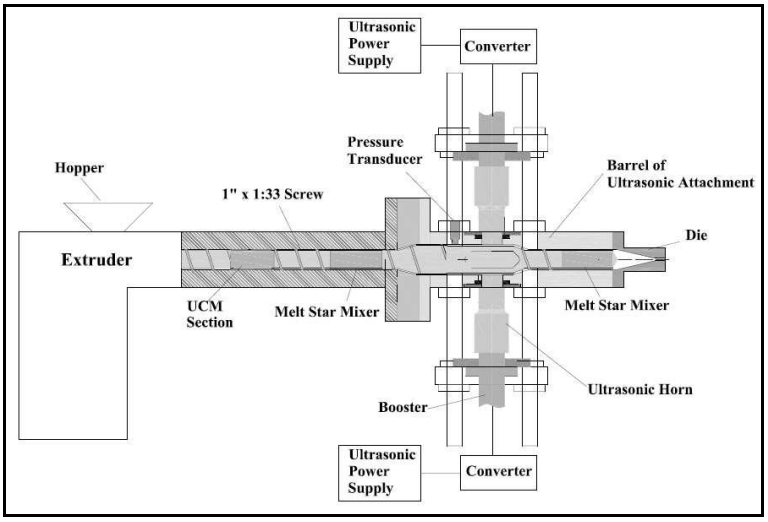

Figure 1. The ultrasonic single screw compounding extruder

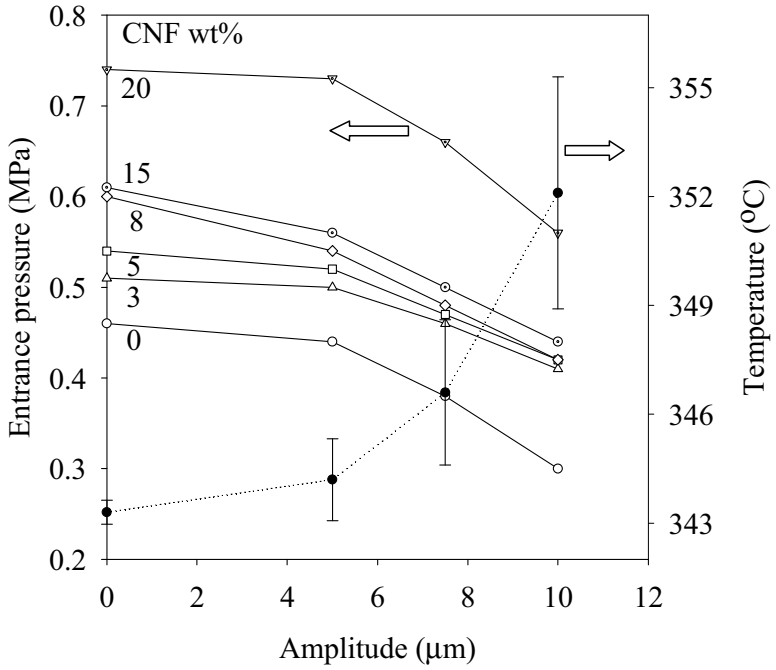

Figure 2. Entrance pressure in front of ultrasonic treatment zone and melt temperature in the ultrasonic treatment zone as a function of amplitude at various CNF concentrations at 60 rpm.

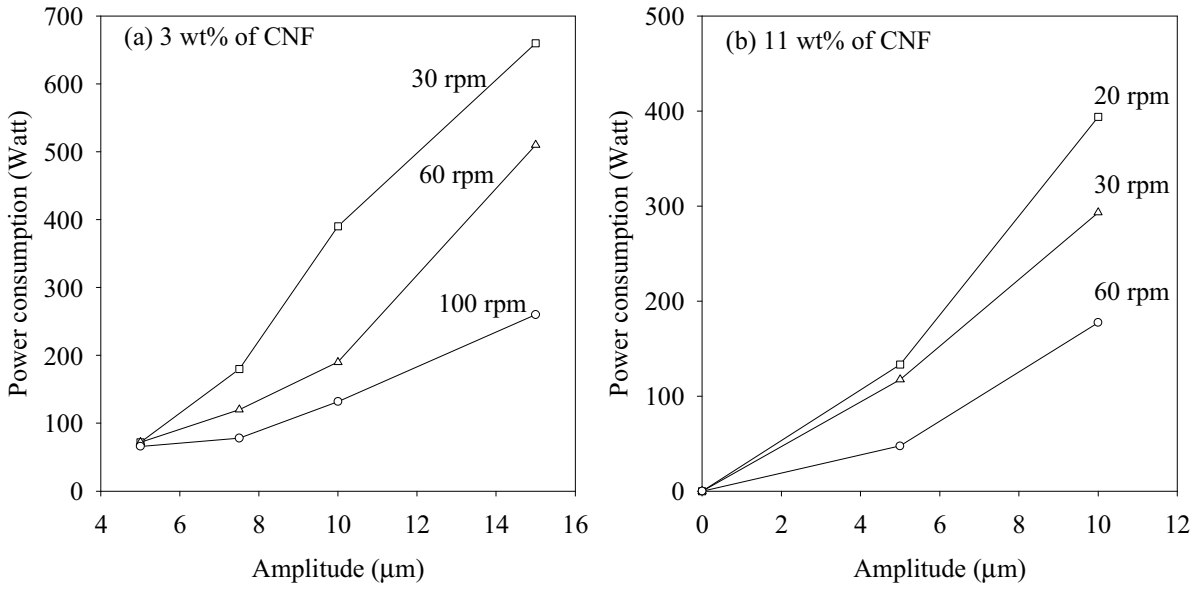

Figure 3. Ultrasonic power consumption as a function of ultrasonic amplitude at flow rate of 15 g/min and various rpm for 3 wt% CNF (a) and 11 wt% CNF (b).

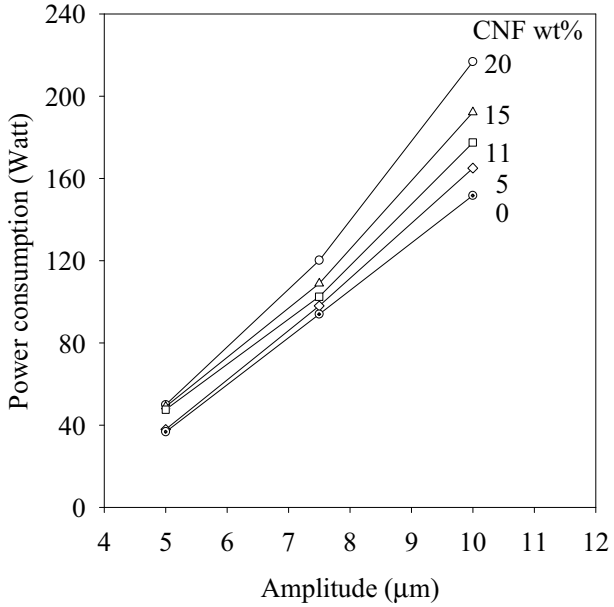

Figure 4. Ultrasonic power consumption as function of ultrasonic amplitude for PEI nanocomposites at various CNF contents at 60 rpm.

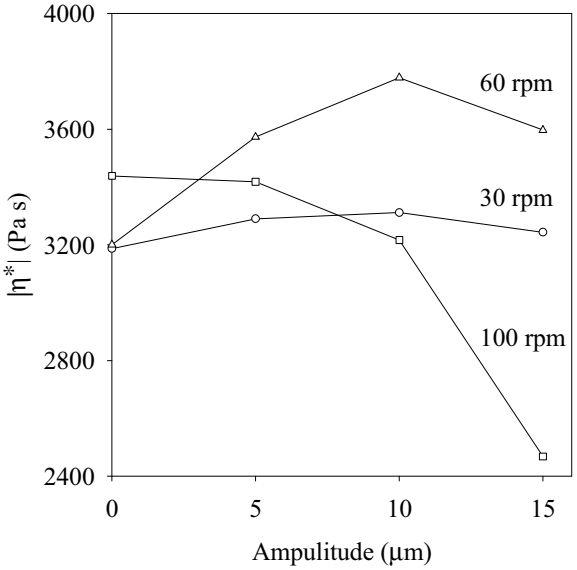

Figure 5. Complex viscosity at frequency of 0.2 s^{-1} as a function of ultrasonic amplitude for 3 wt% CNF /PEI nanocomposites obtained at various screw rpm.

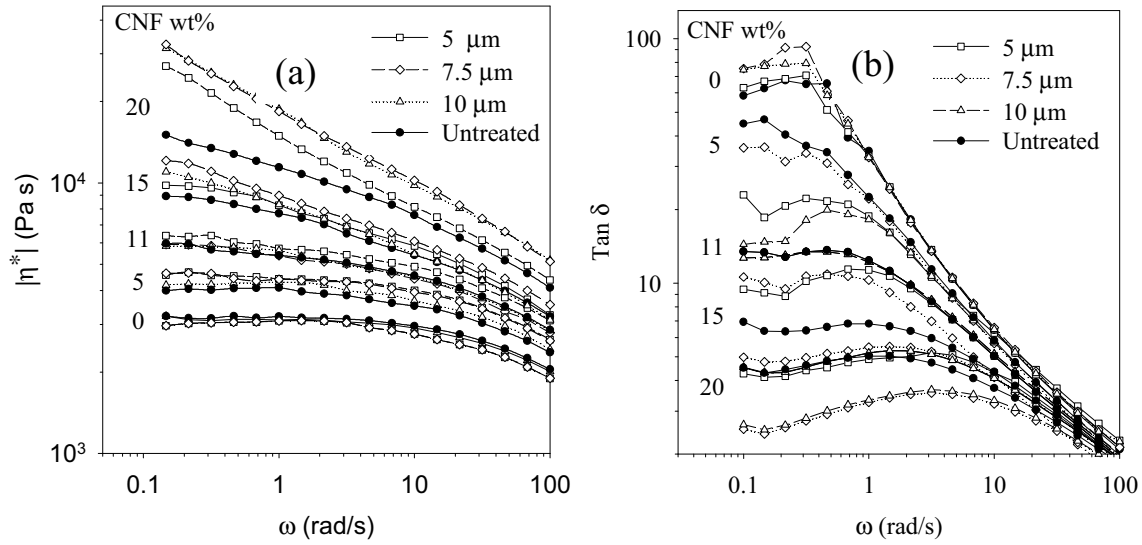

Figure 6. Complex viscosity (a) and Tan δ (b) as a function of frequency for untreated and ultrasonically treated CNF/PEI nanocomposites containing 0 to 20 wt% CNFs obtained at various ultrasonic amplitudes at 60 rpm.

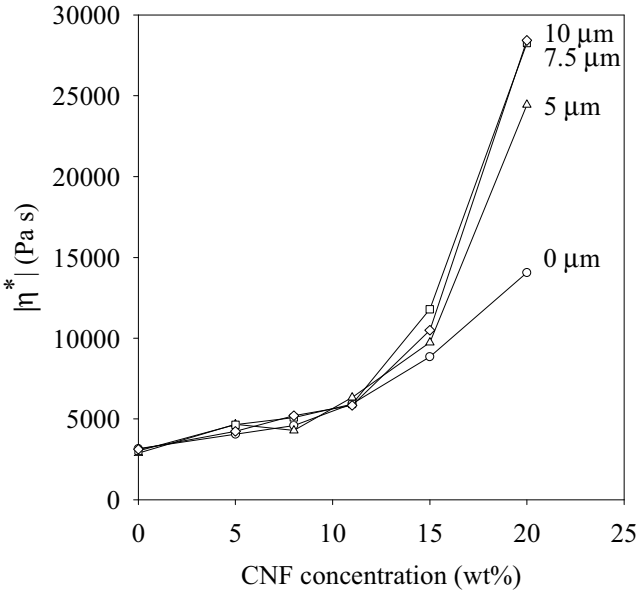

Figure 7. Complex viscosity at a frequency of 0.2 s^{-1} as a function of CNF concentration for untreated and ultrasonically treated composites obtained at various ultrasonic amplitudes at 60 rpm.

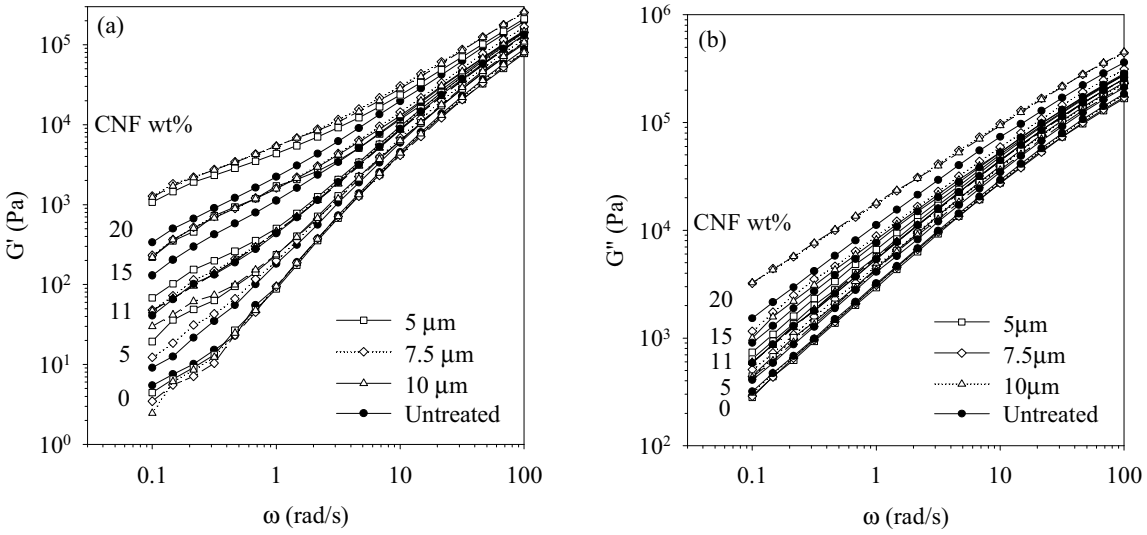

Figure 8. Storage G' (a) and loss G" (b) moduli as a function of frequency for untreated and ultrasonically treated CNF/PEI nanocomposites containing 0 to 20 wt% CNF obtained at various ultrasonic amplitudes at 60 rpm.

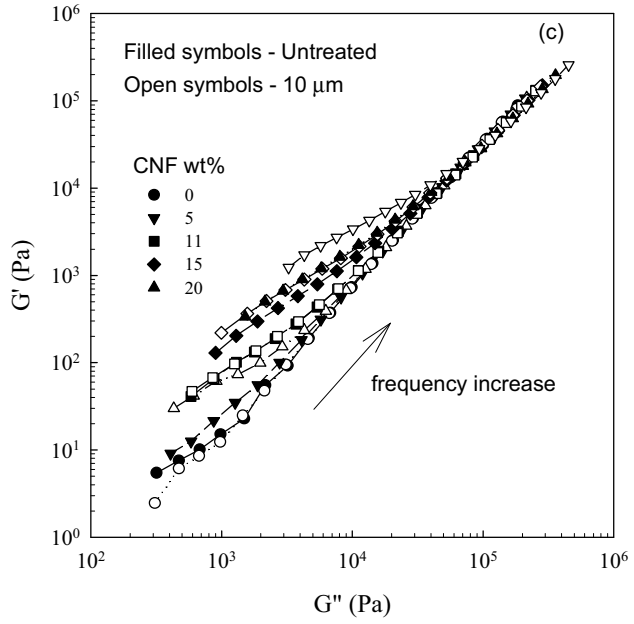

Fig. 8 (c). Storage modulus versus loss modulus for ultrasonically treated and untreated nanocomposites at different carbon nanofibers concentrations.

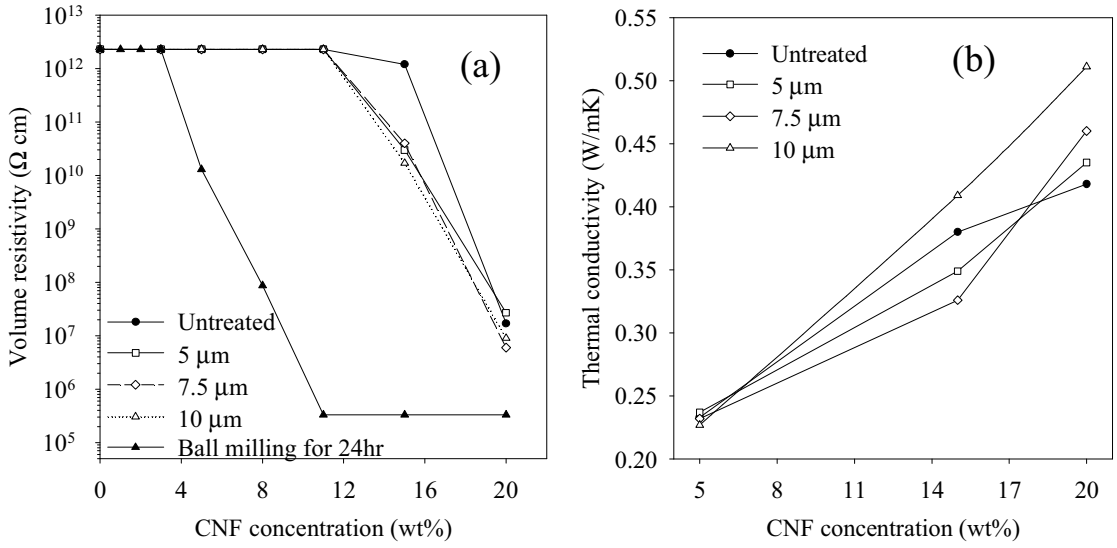

Figure 9. Volume resistivity (a) and thermal conductivity (b) of nanocomposites as a function of CNF concentration obtained at various ultrasonic amplitudes at 60 rpm.

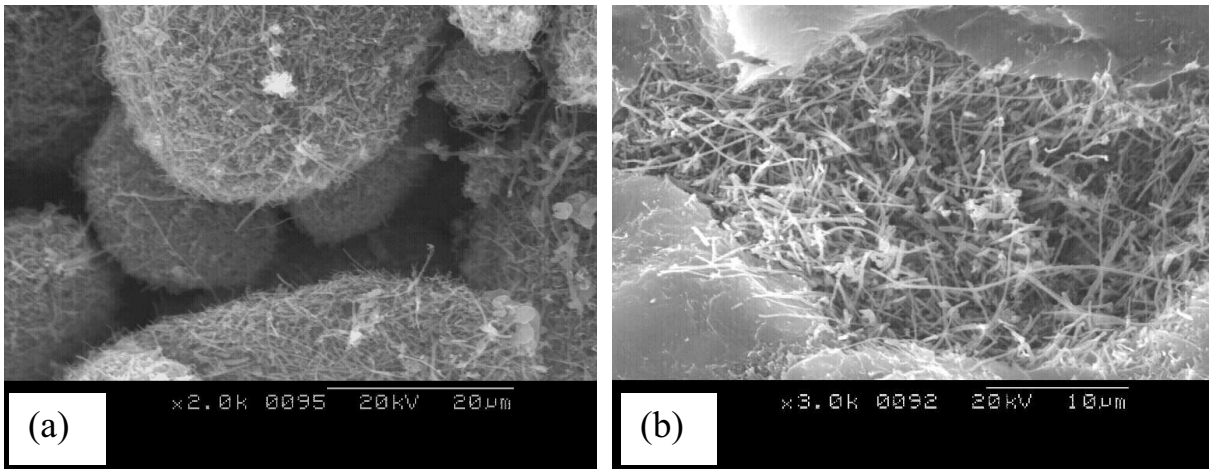

Figure 10. SEM micrographs of CNFs as received (a) and cryofractured surface of nanocomposite containing 3 wt% CNFs prepared by ball mill milling and injection molding (b).

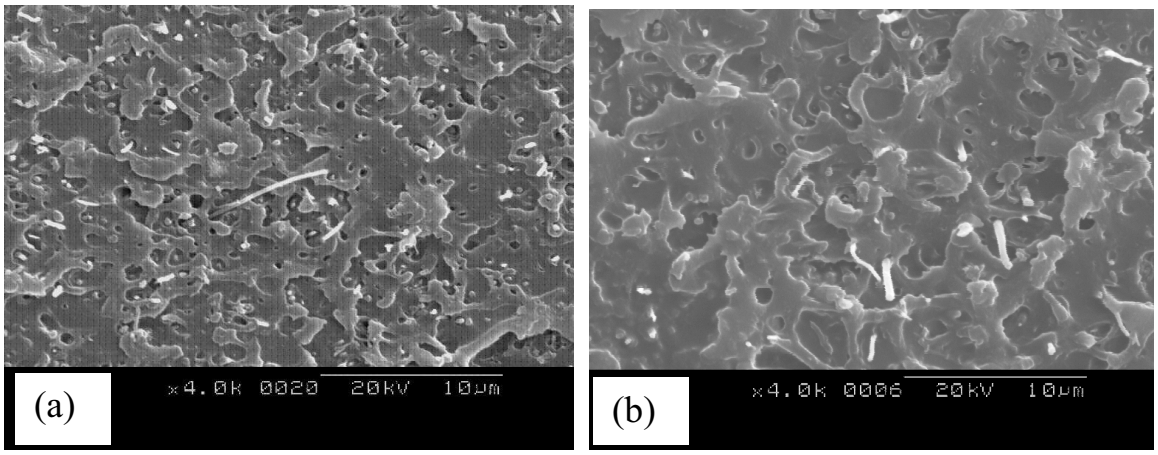

Figure 11. SEM micrographs of cryofractured surface of injection molding of 3 wt% CNF/PEI composites obtained without (a) and with (b) ultrasonic treatment at an amplitude of 10 μm at 60 rpm.

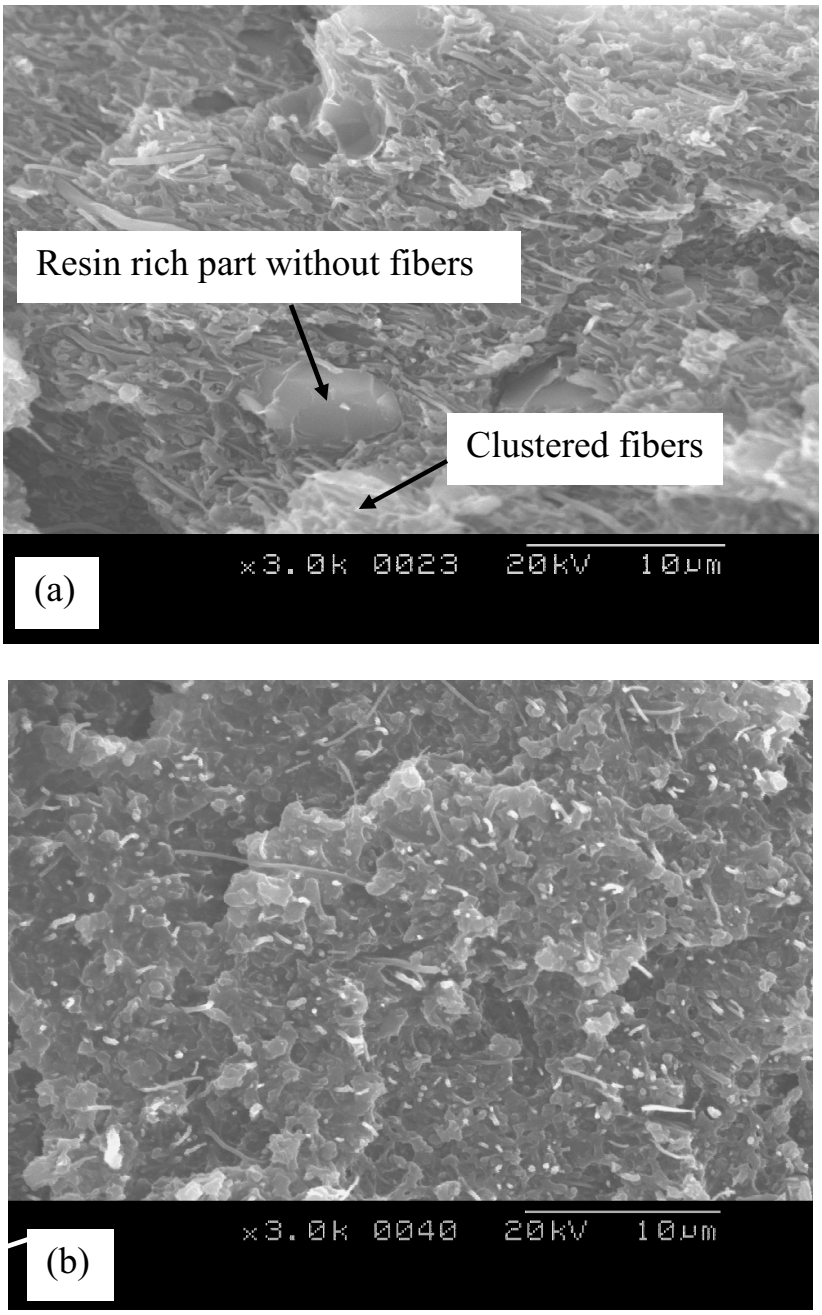

Figure 12. SEM micrographs of cryofractured surface of injection molding of 15 wt% CNF/PEI nanocomposites obtained without (a) and with (b) ultrasonic treatment at an amplitude of 10 µm at 60 rpm.

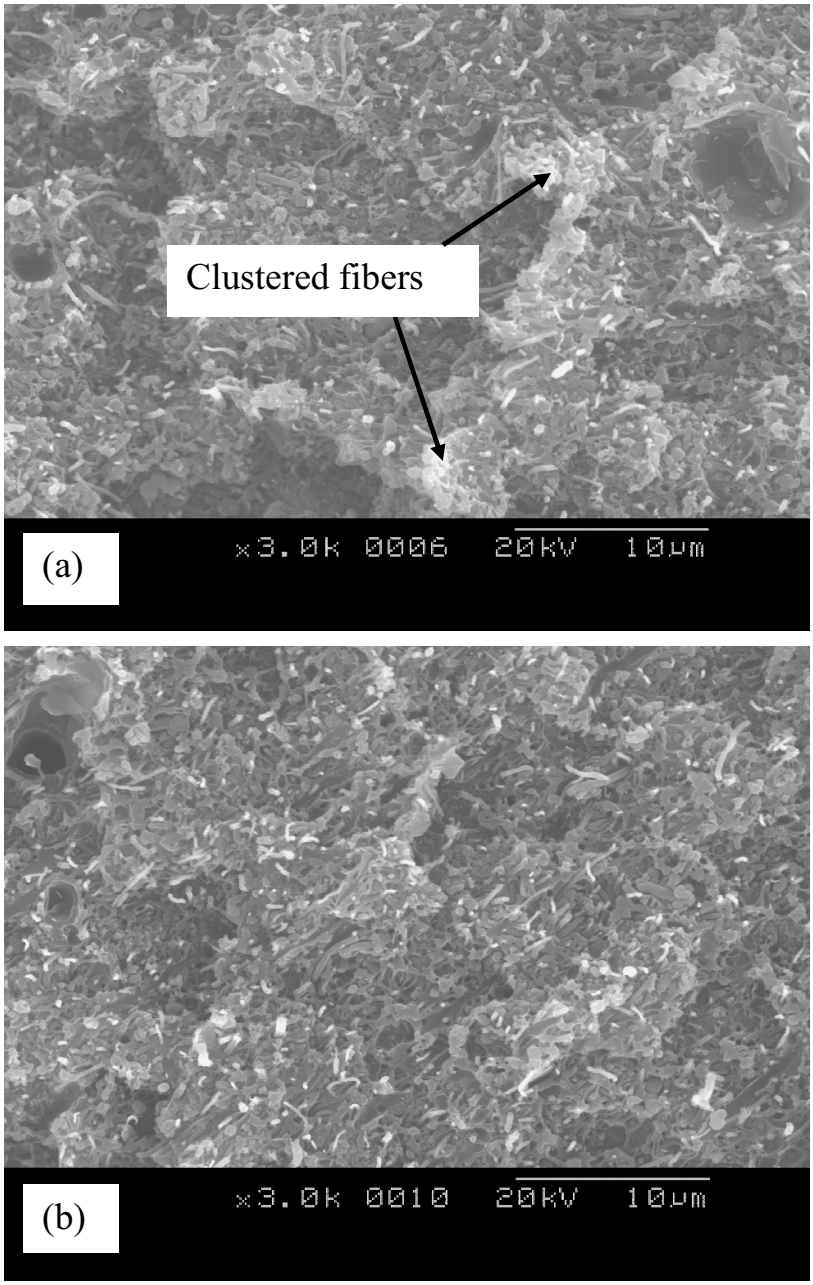

Figure 13. SEM micrographs of cryofractured surface of injection molding of 20 wt% CNF/PEI nanocomposites obtained without (a) and with (b) ultrasonic treatment at an amplitude of 10 µm at 60 rpm.

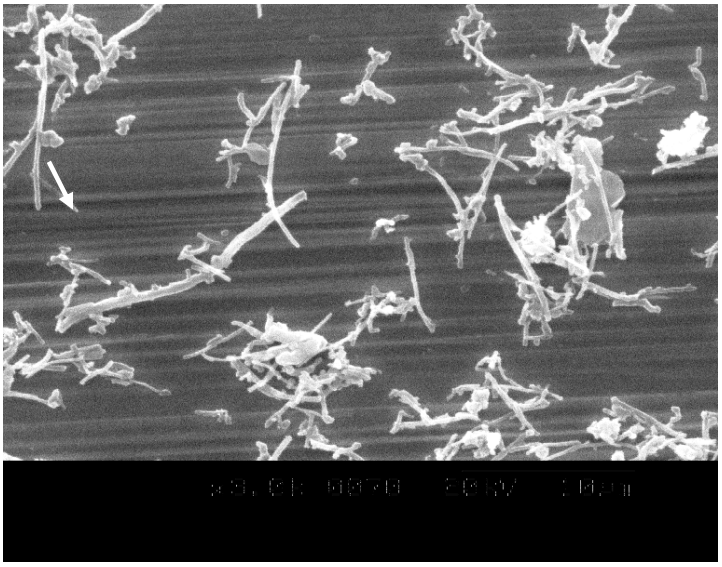

Figure 14. SEM micrographs of CNFs extracted from untreated 11 wt% CNF/PEI nanocomposites at 60 rpm.

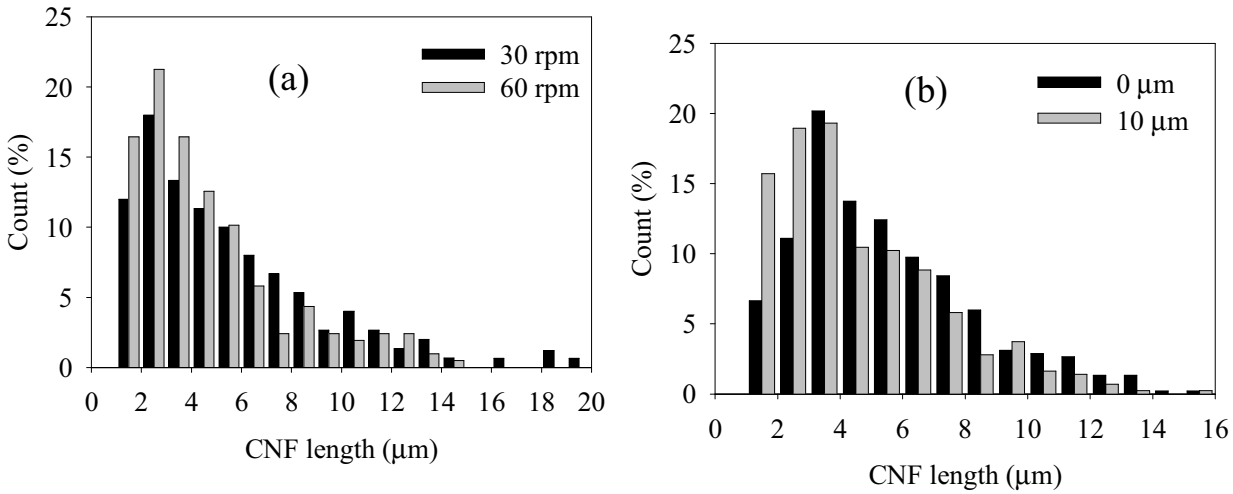

Figure 15. Effect of screw rpm on length distribution of CNFs for 11 wt% CNF/PEI nanocomposites without ultrasonic treatement (a) and effect of ultrasound on length distribution of CNFs for 15 wt% CNF/PEI nanocomposites at 60 rpm (b).

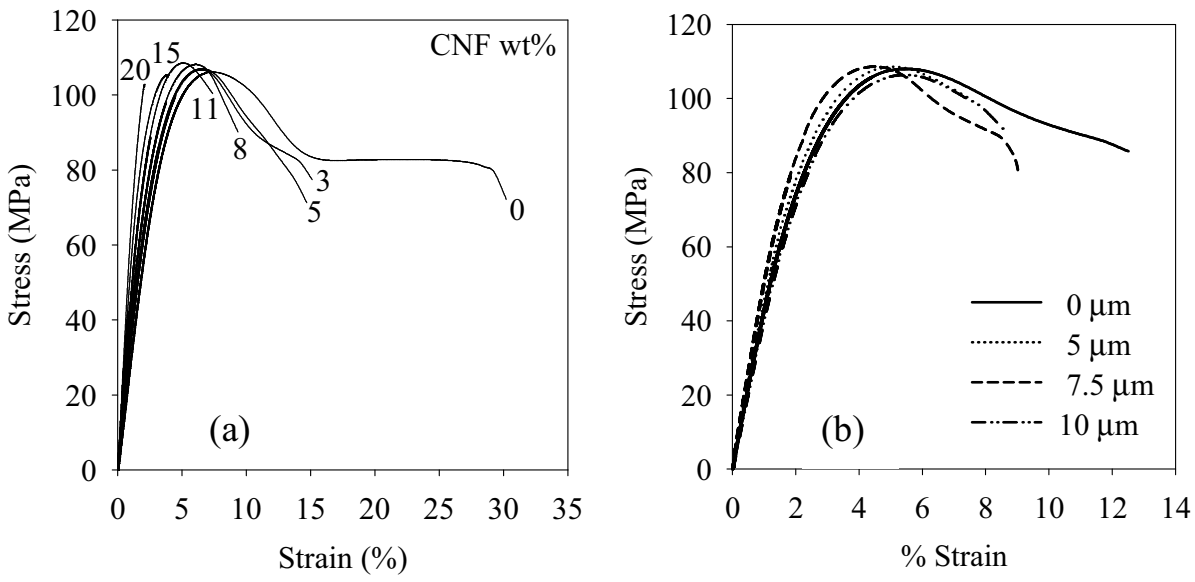

Figure 16. Stress vs. strain curves of CNF/PEI nanocomposites ultrasonically treated at an amplitude of 5 µm at various concentrations (a) and 11wt% PEI/CNF nanocomposites obtained without and with ultrasonic treatment at different amplitudes (b) at 60 rpm.

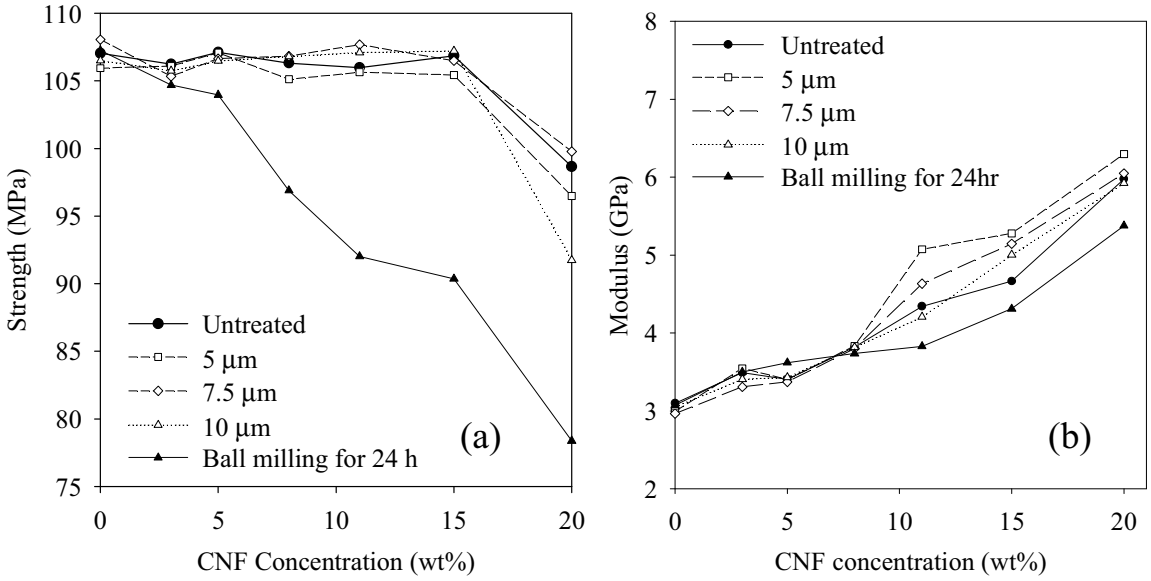

Figure 17. Strength (a) and Young's modulus (b) vs. CNF concentration of CNF/PEI nanocomposites obtained without and with ultrasonic treatment at different amplitudes at 60 rpm and after ball milling.

Table 1. Mechanical properties of PEI/CNF composites

CNF (wt%)	Ultrasonic Amplitute (μm)	Strength (MPa)	Modulus (GPa)	Elongation at yield (%)	Elongation at break (%)	Thoughness (MPa)
0	0	107.03 ± 1.7	3.10 ± 0.2	7.34 ± 0.2	25.20 ± 5.4	20.05 ± 4.5
	5	105.94 ± 1.6	2.99 ± 0.2	7.27 ± 0.3	29.20 ± 9.2	22.52 ± 5.6
	7.5	108.05 ± 1.6	2.96 ± 0.2	7.23 ± 0.0	22.49 ± 7.2	19.25 ± 6.4
	10	108.15 ± 1.7	3.06 ± 0.1	7.35 ± 0.2	21.99 ± 1.8	18.57 ± 1.6
3	0	106.23 ± 1.9	3.49 ± 0.2	6.91 ± 1.3	13.58 ± 6.6	11.98 ± 4.5
	5	106.1 ± 1.8	3.55 ± 0.2	6.59 ± 0.4	14.25 ± 2.4	12.11 ± 2.5
	7.5	105.34 ± 2.1	3.31 ± 0.2	6.48 ± 0.3	13.54 ± 3.5	11.29 ± 3.3
	10	105.74 ± 1.5	3.41 ± 0.1	6.46 ± 0.2	13.33 ± 3.0	11.02 ± 2.6
5	0	107.11 ± 0.8	3.41 ± 0.1	6.41 ± 0.4	14.11 ± 4.9	11.98 ± 4.5
	5	107.08 ± 1.6	3.41 ± 0.1	6.30 ± 0.4	13.02 ± 3.7	13.02 ± 3.8
	7.5	106.65 ± 1.0	3.38 ± 0.2	6.43 ± 0.1	14.09 ± 2.5	11.98 ± 2.2
	10	106.48 ± 2.3	3.43 ± 0.1	6.40 ± 0.5	16.73 ± 2.9	14.06 ± 2.2
8	0	106.32 ± 1.0	3.82 ± 0.2	5.63 ± 0.0	9.66 ± 1.2	8.10 ± 1.0
	5	105.12 ± 5.6	3.83 ± 0.2	5.38 ± 1.1	7.76 ± 2.6	7.47 ± 1.4
	7.5	106.84 ± 2.3	3.80 ± 0.1	5.70 ± 0.5	13.27 ± 5.0	11.86 ± 3.4
	10	106.81 ± 0.9	3.82 ± 0.3	5.72 ± 0.3	11.15 ± 4.9	9.44 ± 4.6
11	0	105.98 ± 3.2	4.34 ± 0.2	5.17 ± 0.4	11.42 ± 2.9	11.50 ± 1.2
	5	105.64 ± 5.8	5.07 ± 0.5	4.36 ± 0.9	8.53 ± 5.0	8.56 ± 3.7
	7.5	107.68 ± 1.5	4.63 ± 0.5	5.01 ± 0.4	8.77 ± 1.3	7.53 ± 1.3
	10	107.1 ± 1.5	4.21 ± 0.2	5.10 ± 0.3	8.73 ± 2.4	7.35 ± 2.4
15	0	106.86 ± 5.7	4.66 ± 0.2	3.98 ± 0.7	4.32 ± 1.3	3.23 ± 1.4
	5	105.44 ± 2	5.28 ± 0.2	3.84 ± 0.4	3.95 ± 0.5	2.87 ± 0.5
	7.5	106.49 ± 4.6	5.14 ± 0.2	4.03 ± 0.8	4.06 ± 0.8	2.99 ± 0.8
	10	107.21 ± 3.1	5.01 ± 0.3	3.97 ± 0.6	4.24 ± 1.0	3.23 ± 1.0
20	0	98.67 ± 8.0	5.97 ± 0.3	2.05 ± 0.4	2.05 ± 0.4	1.18 ± 0.4
	5	96.49 ± 6.0	6.29 ± 0.2	1.89 ± 0.3	1.89 ± 0.3	1.06 ± 0.3
	7.5	99.78 ± 6.9	6.05 ± 0.2	2.12 ± 0.3	2.18 ± 0.3	1.30 ± 0.3
	10	91.74 ± 7.6	5.93 ± 0.5	1.85 ± 0.3	1.85 ± 0.3	0.96 ± 0.3